RESEARCH ARTICLE

ScienceAsia 35 (2009): **80–88**

doi: 10.2306/scienceasia1513-1874.2009.35.080

Automatic exudate detection for diabetic retinopathy screening

Akara Sopharak[a,*], **Bunyarit Uyyanonvara**[a], **Sarah Barman**[b]

[a] Department of Information Technology, Sirindhorn International Institute of Technology, Thammasat University, 131 Moo 5, Tiwanont Road, Bangkadi, Muang, Pathumthani 12000, Thailand

[b] Faculty of Computing, Information Systems and Mathematics, Kingston University, Penrhyn Road, Kingston upon Thames, Surrey, KT1 2EE, UK

[*] Corresponding author, e-mail: akara@siit.tu.ac.th

Received 8 Sep 2008
Accepted 12 Feb 2009

ABSTRACT: Exudates are one of the primary signs of diabetic retinopathy which is a main cause of blindness that could be prevented with an early screening process. Pupil dilation is required in the normal screening process but this affects patients' vision. Automatic computerized screening could facilitate the screening process, reduce inspection time, and increase accuracy. In this paper we propose an automatic method to detect exudates from low-contrast digital images of retinopathy patients with non-dilated pupils using a fuzzy c-means (FCM) clustering technique. Preprocessing of contrast enhancement was applied in order to enhance the quality of the input image before four features, namely, intensity, standard deviation on intensity, hue, and number of edge pixels, were selected to supply to the FCM method. The number of required clusters was optimally selected from a quantitative experiment where it was varied from two to eight clusters. The number of cluster optimization was based on sensitivity and specificity which were calculated by comparison of the detected results and hand-drawn ground truths from expert ophthalmologists. The positive predictive value and positive likelihood ratio were also used to evaluate the overall performance of this method. From the result of the subtracted cluster with the number of clusters equalling 2, it was found that the proposed method detected exudates with 92.18% sensitivity and 91.52% sensitivity.

KEYWORDS: non-dilated retinal images, fuzzy c-means clustering, medical image processing

INTRODUCTION

Blindness is an outcome of diabetic retinopathy and its prevalence is set to continue rising. An estimated 50–65 new cases of blindness per 100 000 occurs every year[1]. The screening of diabetic patients for the development of diabetic retinopathy can potentially reduce the risk of blindness in these patients by 50%[2–6]. Early detection enables laser therapy to be performed to prevent or delay visual loss and may be used to encourage improvement in diabetic control. Current methods of detection and assessment of diabetic retinopathy are manual, expensive, and require trained ophthalmologists.

Sinthanayothin et al[3,4] reported the result of an automated detection of diabetic retinopathy on digital fundus images using a recursive region growing segmentation (RRGS) algorithm on a 10×10 window. In the preprocessing step, adaptive, local, contrast enhancement was applied. The optic disc, blood vessels, and fovea detection were also localized. Sanchez et al[5] combined colour and sharp edge features to detect the exudates. The yellowish objects were detected first; the objects in the image with sharp edges were then detected using Kirsch's mask and different rotations of it on the green component. The combination of results of yellowish objects with sharp edges was used to determine the exudates. Hsu et al[6] presented a domain knowledge based approach to detect exudates. A median filter was used to compute an intensity difference map. Dynamic clustering was then used to determine lesion clusters. Finally, domain knowledge was applied to identify true exudates. Gardner et al[7] proposed an automatic detection of diabetic retinopathy using an artificial neural network. The exudates were identified from grey-level images and the fundus image was analysed using a back-propagation neural network. The classification of a 20×20 region was used rather than a pixel-level classification. Wang et al[8] used colour features on a Bayesian statistical classifier to classify each pixel into lesion or non-lesion classes. Walter et al[9] detected exudates using grey-level variation and contours determined by means of morphological reconstruction techniques.

Phillips et al[10] applied a thresholding technique based on the selection of regions to detect exudates. A patch of size 256×192 pixels was selected over the area of interest. Global thresholding was used to detect the large exudates while local thresholding was used to detect the lower intensity exudates. Huiqi and Chutatape[11] proposed an exudate extraction technique by using a combination of region growing and edge detection techniques. The optic disc was also detected in this paper by principal component analysis. The shape of the optic disc was then detected using a modified active shape model. Usher et al[12] detected the candidate exudate regions by using a combination of RRGS and adaptive intensity thresholding. The candidate regions were extracted using size, shape, hue, and intensity features. Then these features were used as the input to a neural network. Kavitha and Devi[13] proposed three steps to detect exudates. Median filtering and morphological operation were used to detect blood vessels. Multilevel thresholding was used to extract the bright regions in a second step. The convergent point of blood vessels was used to detect the optic disc and finally, further bright regions were assigned as exudates. Goh et al[14] used the minimum distance discriminant to detect the exudates. The spectrum feature centre of exudates and background were computed and then the distance from each pixel to the class centre was calculated. The pixel was classified as exudate if it fell within the minimum distance. Ege et al[15] used a median filter to remove noise. Bright lesions and dark lesions were separated by thresholding. A region growing algorithm was used to locate exudates. Bayesian, Mahalanobis, and kNN classifiers were tested. From these experiments, the Mahalanobis classifier was shown to yield the best result.

Fuzzy c-means (FCM) clustering is a well-known clustering technique for image segmentation[16–18]. It was developed by Dunn[19] and improved by Bezdek[20]. It has also been used in retinal image segmentation[21–24]. Osareh et al[21] used colour normalization and a local contrast enhancement in a pre-processing step. The colour retinal images were segmented using FCM clustering and the segmented regions were classified into two disjoint classes of exudate and non-exudate patches using a neural network[22]. The feature set used for training the neural network consisted of size, colour, average intensity, edge sharpness, and standard deviation of intensity. The mean and standard deviation of Luv values, compactness, and Luv values of region centroid were added to be features of the neural network. The same authors also located the optic disc using template matching, least squares regression arc estimation, and snakes[23]. A comparative exudate classification using Support Vector Machines (SVMs) and neural networks was also applied[24]. They showed that SVMs were more practical than the others. Zhang and Chutatape[25] used local contrast enhancement preprocessing and Improved FCM (IFCM) in Luv colour space to segment candidate bright lesion areas. IFCM was applied in two stages, first in L, u, and v colour space. Then in the second step, the components u and v were used to distinguish bright lesions and background. A hierarchical SVMs classification structure was applied to classify bright non-lesion areas, exudates, and cotton wool spots.

Most of the techniques mentioned above worked on images taken when the patient had dilated pupils in which exudates and other retinal features are clearly visible. In a normal diabetic retinopathy screening process, pupils are dilated using tropicamide 1% eye drops. The process takes about 15–20 minutes to work and has an effect on the patient. The dilating drops may impair focusing of the eyes for several hours and produce a brief stinging sensation, nausea, vomiting, dryness of the mouth, and dizziness. The examination time and effect on the patient could be reduced if the system could work on images taken where the pupil of the patient is not dilated.

In this paper, we present an automatic method to detect exudates from low quality retinal images taken from non-dilated pupils from diabetic retinopathy patients using a FCM clustering algorithm. The number of resulting clusters was optimized, based on the accuracy of values when compared with clinicians' hand-drawn ground truth.

EXUDATE DETECTION

Forty digital retinal images from 32 patients were obtained from a KOWA-7 non-mydriatic retinal camera with a 45° field of view taken at Thammasat University hospital. The images were stored in JPEG image format files with the lowest compression rates. The image size used was 500×752 pixels with 24 bit colour.

Exudates can be identified on the ophthalmoscope as white or yellowish areas with varying sizes, shapes, and locations. They normally appear near the leaking capillaries within the retina. The main cause of exudates is proteins and lipids leaking from the blood into the retina via damaged blood vessels[22–26]. This part of the paper describes how features were selected to be used in a segmentation process using FCM clustering and also explains how the number of clusters was optimized.

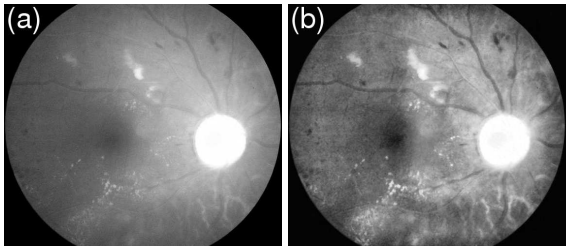

Fig. 1 Pre-processing result: (a) original I band (b) I band after pre-processing.

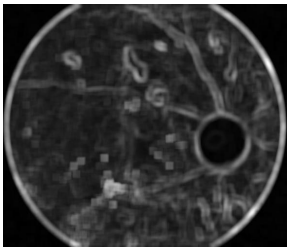

Fig. 2 Standard deviation result: standard deviation of Fig. 1b.

Feature Extraction

Four features were experimentally extracted as input for FCM clustering. They were the intensity value after pre-processing, the standard deviation of intensity, the hue, and the number of edge pixels from an edge image.

The intensity of the image after pre-processing (I_{CLAHE}) was selected as one of the classification features because exudate pixels can usually be distinguished from normal pixels by their intensity.

Firstly, the red, green, and blue (RGB) space in the original image was transformed to hue, saturation, and intensity (HSI) space. A median filtering operation was then applied on the I band to reduce noise before a contrast-limited adaptive histogram equalization (CLAHE) was applied for contrast enhancement. CLAHE operates on small regions in the image. The contrast of each small region is enhanced with histogram equalization[27]. The original intensity band image and intensity band after preprocessing are shown in Figs. 1a and b, respectively.

The standard deviation of I_{CLAHE} (σ) was also chosen as an input parameter because the distribution measurement of the pixel values would differentiate the exudate area from the others since standard deviation shows the main characterization of the closely distributed cluster of exudates. It is defined by

$$\sigma(x) = \frac{1}{N-1} \sum_{i \in W(x)} (I_{\mathrm{CLAHE}}(i) - \mu_{I_{\mathrm{CLAHE}}}(x))^2,$$

where x is a set of all pixels in a sub-window $W(x)$, N is the number of pixels in $W(x)$, $\mu_{I_{\mathrm{CLAHE}}}(x)$ is the mean value of $I_{\mathrm{CLAHE}}(i)$, and $i \in W(x)$. A window size of 15×15 pixels was used in this step. The standard deviation of the intensity bands after preprocessing is shown in Fig. 2b.

Hue, also extracted from HSI space, was the third feature selected because hue components make up chrominance or colour information. The exudates are either yellowish or white. The original RGB image (shown in grey) and the hue image are shown in Figs. 3a and b, respectively.

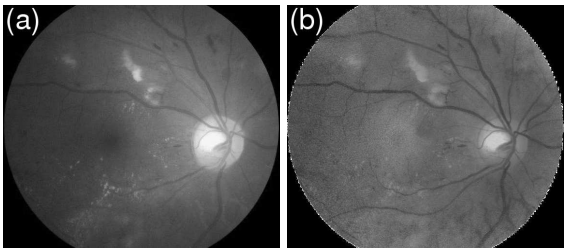

Fig. 3 Hue result: (a) original RGB image (b) hue image.

Normally exudates gather together in small clusters so they tend to have many edge pixels around the area. That is the reason why a number of edge pixels were selected as our last feature. However, during this feature extraction, we removed some irrelevant edge pixels, as described in the following algorithm.

Step 1: For fast edge detection, a Sobel edge operator with a mask size of 3×3 pixels was used to compute the gradient magnitude.

Step 2: The result from the previous step was then thresholded by a fixed low value in order to get most of the edge pixels.

Step 3: Some of the resulting edge pixels from the previous step do not represent the edge of the exudates. Some of them are part of the edge of the vessel, and these vessel edge pixels need to be removed before proceeding to the next step. Quick and approximate blood vessel detection was achieved by using a decorrelation stretch on the red band. Decorrelation stretching is a process used to enhance (or 'stretch') the colour differences found in a colour image. Contrast exaggeration was used to expand the range of intensities of highly correlated images. Exaggeration of the least correlated portion of the data can be used to enhance the colour in highly correlated images in order to decrease the correlation of the data[28,29]. The scatter plot of the RGB image and the RGB image after decorrelation stretching

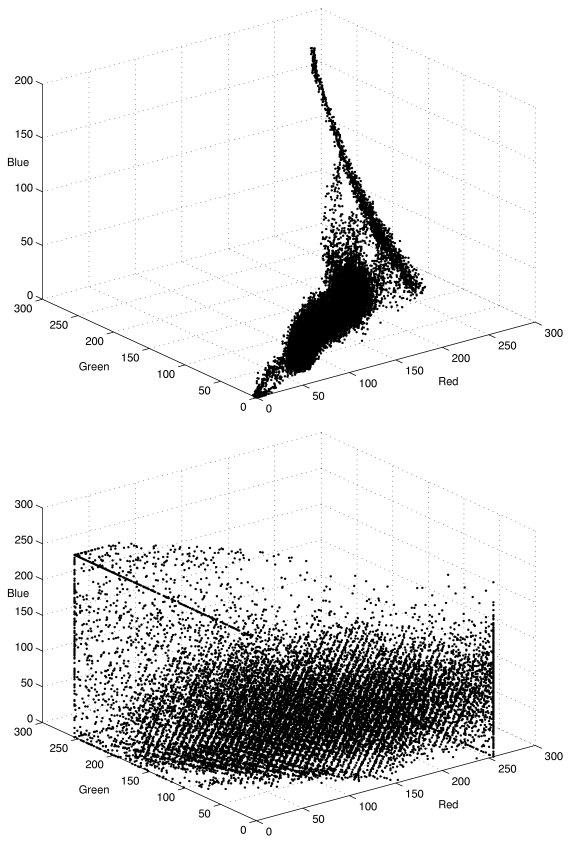

Fig. 4 Scatter plot of (a) RGB image (b) RGB image after decorrelation stretch (1 in every 5 points plotted).

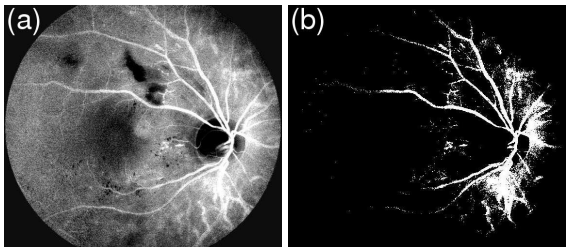

Fig. 5 Blood vessel detection: (a) decorrelation stretch image on red plane (b) blood vessel detected from decorrelation stretch image.

is shown in Fig. 4. The scatter plot of the image shows how the bands are decorrelated and equalized. The scatter plot of the RGB image indicates that the visible planes are highly correlated while a scatter plot of the RGB image after decorrelation stretching shows a strong decrease in correlation. Blood vessels can be detected by thresholding this result and the detection results are shown in Fig. 5.

Step 4: Some exudates are soft exudates which cannot be detected by a strong edge. High-value red pixels selected from the decorrelation stretch image were chosen and added to the result from the previous step because the soft exudates normally appear red. However, red pixels which belong to the optic disc, which also appear red, have to be removed first. The optic disc was quickly detected by using an entropy feature on I_{CLAHE}. The entropy is a statistic measurement of randomness that can be used to characterize the texture of the input image. Entropy is defined as

$$H(x) = -\sum_{i \in W(x)} p_i \log_2 p_i,$$

where x is a set of all pixels in a sub-window $W(x)$, p_i is the histogram count in sub-window i. A window size of 9×9 pixels was used in this step.

The optic disc which is normally smooth appears in relatively low intensity in entropy space. The resulting image was thresholded at an automatically selected grey level, using the Otsu algorithm. To ensure that all the neighbouring pixels of the thresholded result were also included in the candidate region, a binary dilation operator was also applied. For this step, a flat disc-shaped structuring element with a fixed radius of 11 was used. An example result of an entropy space image and an image with all the optic disc area masked out are shown in Figs. 6a and b, respectively.

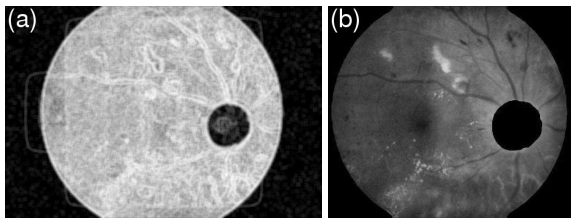

Fig. 6 Optic disc detection: (a) entropy image (b) optic disc area eliminated from the contrast-enhanced image.

Step 5: A number of neighbouring white pixels of the resulting image from Steps 1–4 was counted using a window size of 17×17 to form our final feature, namely, an image of the edge pixels (Fig. 7).

These four features will be used in the segmentation process as described in the next section.

Segmentation using FCM clustering

FCM clustering is an overlapping clustering algorithm. Each point may belong to two or more clusters with different degrees of membership. Features with a high similarity in an image are grouped into the

Fig. 7 Image of edge pixels.

same cluster. The similarity is quantified in terms of the distance of the feature vector to the cluster centre. Euclidean distance is used to measure this distance and the input data will be associated with an appropriate membership value[25,30,31]. The cluster centre is updated until the difference between the objective function at successive iterations is less than a criterion assigned previously. The objective function is given by

$$J = \sum_{i=1}^{M}\sum_{j=1}^{C} u_{ij}^2 \|x_i - c_j\|^2, \tag{1}$$

$$u_{ij} = \left[\sum_{k=1}^{c}\left(\frac{\|x_i - c_j\|}{\|x_i - c_k\|}\right)^2\right]^{-1}, \tag{2}$$

$$c_j = \frac{\sum_{i=1}^{M} u_{ij}^2 x_i}{\sum_{i=1}^{M} u_{ij}^2}, \tag{3}$$

where M is the number of features (four in our case), C is the number of clusters (in our case, experimentally varying from two to eight), u_{ij} is the degree of membership of x_i in the cluster j, x_i is the ith item of the d-dimensional measured data, c_j is the centre of the cluster, and $\|*\|$ is any norm expressing the similarity between any measured feature and the centre.

Fuzzy partitioning is carried out through an iterative optimization of the objective function by updating u_{ij} and c_j. The iteration stops when

$$\max_{ij}\left\{|u_{ij}^{(k+1)} - u_{ij}^{(k)}|\right\} < \varepsilon, \tag{4}$$

where ε was set at 0.00001 in our case, and k is the iteration number (set to a maximum of 200 in our case). This procedure converges to a local minimum or a saddle point of J.

The input to the FCM algorithm is as follows.

Step 1: Initialize the fuzzy partition matrix $U = [u_{ij}]$ ($U^{(0)}$) by generating random numbers in the range 0 to 1 subject to

$$\sum_{i=1}^{M}\sum_{j=1}^{C} u_{ij} = 1$$

and set $k = 0$.

Step 2: Calculate the centres vectors $C^{(k)} = [c_j]$ with $U^{(k)}$ according to (3).

Step 3: Obtain $U^{(k+1)}$ by using the newly computed u_{ij} according to (2).

Step 4: Compute J according to (1). If (4) is satisfied, stop. Otherwise, return to step 2.

The output from the FCM clustering algorithm is a list of cluster centres and n membership-grades for each pixel, where n is the number of desired clusters. A pixel will be assigned to the cluster with highest membership-grade. However, the problem of using the FCM clustering technique is that the numbers of desired clusters, n, has to be specified beforehand. To determine the suitable value of n, we tried values ranging from 2 to 8. In each case the FCM clustering algorithm was applied to 40 test images (making 35 clusters in total for each image). The results for images using $n = 2$ and $n = 8$ are shown in Fig. 8 and 9, respectively.

Performance measurement

The performance of each parameter was measured by comparing the detection result with ophthalmologists' hand-drawn ground truth and various performance measurements[32,33]. We first define N_{TP} as the number of exudate pixels correctly classified (true positive), N_{FP} as the number of non-exudate pixels which are incorrectly classified as exudate pixels (false positive), N_{FN} as the number of exudate pixels that were not detected (false negative), and N_{TN} as the number of non-exudate pixels correctly classified (true negative). The sensitivity (or true positive rate) is

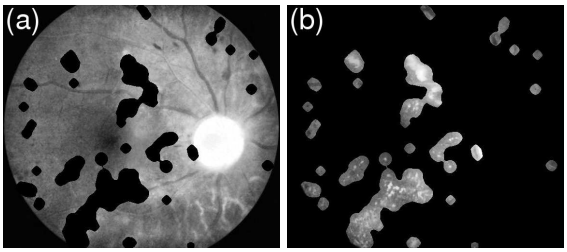

Fig. 8 FCM clustering results with $n = 2$: (a) Cluster 1 (b) Cluster 2.

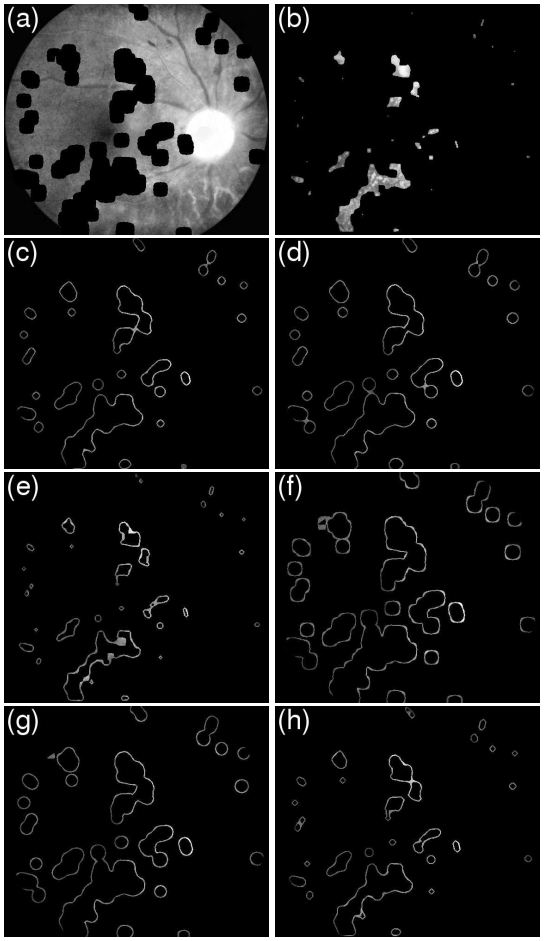

Fig. 9 FCM clustering results with $n = 8$: (a) to (h) are Clusters 1 to 8.

the proportion of exudate pixels which are positively detected and is hence given by

$$\text{Sensitivity} = \frac{N_{\text{TP}}}{N_{\text{TP}} + N_{\text{FN}}}.$$

It is a measure of how well the test detects exudates when they are present since a lower N_{FN} leads to higher sensitivity. Specificity (or true negative rate) is the proportion of non-exudate pixels which are negatively detected and so

$$\text{Specificity} = \frac{N_{\text{TN}}}{N_{\text{TN}} + N_{\text{FP}}}.$$

It is a measure of how well the test detects non-exudates when they are absent. A system with 100% sensitivity and specificity would be perfect detection system.

The positive predictive value (PPV) is the proportion of exudate and non-exudate pixels which are positively detected and hence

$$\text{PPV} = \frac{N_{\text{TP}}}{N_{\text{TP}} + N_{\text{FP}}}.$$

The positive likelihood ratio (PLR) is given by

$$\text{PLR} = \frac{\text{Sensitivity}}{1 - \text{Specificity}} = \frac{N_{\text{TP}}(N_{\text{TN}} + N_{\text{FP}})}{N_{\text{FP}}(N_{\text{TP}} + N_{\text{FN}})}.$$

The larger the PPV and PLR, the better the performance of the exudate detection system. 95% confidence intervals (CIs) for PPV and PLR were also computed.

RESULTS AND DISCUSSION

Forty images were tested on an AMD Athlon 1.25 GHz PC using MATLAB. The approximate times taken for running the whole process for each image with $n = 2$, 3, 4, 5, 6, 7, and 8 were 1.5, 2, 5, 7, 10.5, 15, and 18 min, respectively.

Two candidate clusters were used as exudate detection results. The first candidate is Cluster 1 (Figs. 8a and 9a). This cluster contains most of the original image information but all exudate areas are missing. In this case, the exudate pixels can be obtained by subtracting this first cluster from the original intensity image to produce what we will refer to as the subtracted cluster, an example which is shown in Fig. 10b. By visual inspection, all the exudate pixels seem to be captured within this result. The result might yield a very high true positive value; however, the false positive value would also be very high too due to misclassified non-exudate pixels.

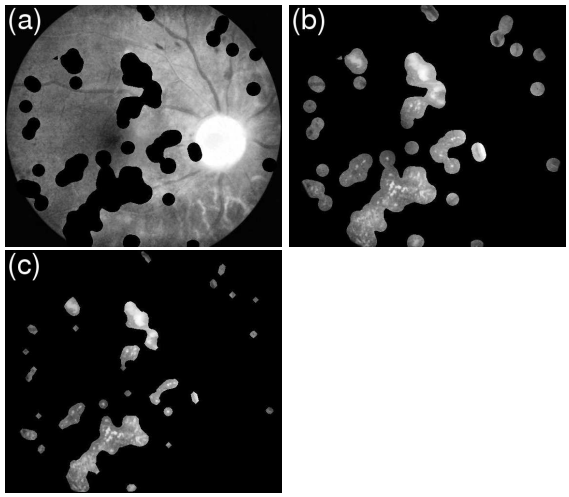

Fig. 10 Candidate clusters with $n = 3$: (a) first cluster (b) subtracted cluster (c) second cluster.

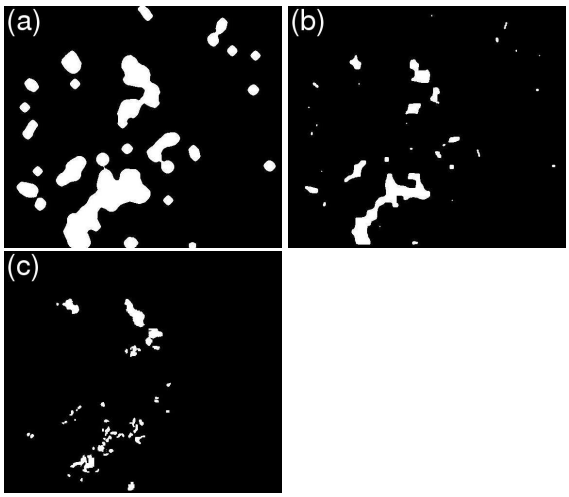

Fig. 11 Comparison of exudate detection: (a) detected result from subtracted cluster with $n = 2$ (b) detected result from second cluster with $n = 8$ (c) ground truth image.

The second important candidate cluster is Cluster 2 which we will refer to as the second cluster. This result has mostly exudate pixels on a black background (Figs. 8b and 9b). Even though this cluster contains fewer pixels, most of them are true exudate pixels which may give a smaller true positive value. However, it also reduces the false positive value because misclassification of non-exudate pixels is also lower. Fig. 10 displays example results of these two candidate clusters. Fig. 11 displays the comparison of exudate detection from the subtracted cluster and the second cluster with the ground-truth image. The exudate detection results of from two images using subtracted cluster and second cluster are shown in Fig. 12.

The performance of our technique was evaluated quantitatively by comparing the result of extractions with ophthalmologists' hand-drawn ground-truth images. This approach aims to measure the correctness of the algorithms at the pixel level.

Using the subtracted cluster, the maximum values of PPV and PLR are 34.20 and 32.70 with $n = 2$, and the minimum values of PPV and PLR are 0.06 and 3.63 with $n = 8$. Using the second cluster, the maximum values of PPV and PLR are 55.20 and 93.99 with $n = 8$, and the minimum values of PPV and PLR are 0.10 and 5.35 with $n = 2$. The detailed results of performance measurement using PPV and PLR of the subtracted and second cluster result are presented in Table 1, and the average values of sensitivity, specificity, 95% CI of PPV, and 95% CI of PLR for are given in Table 2.

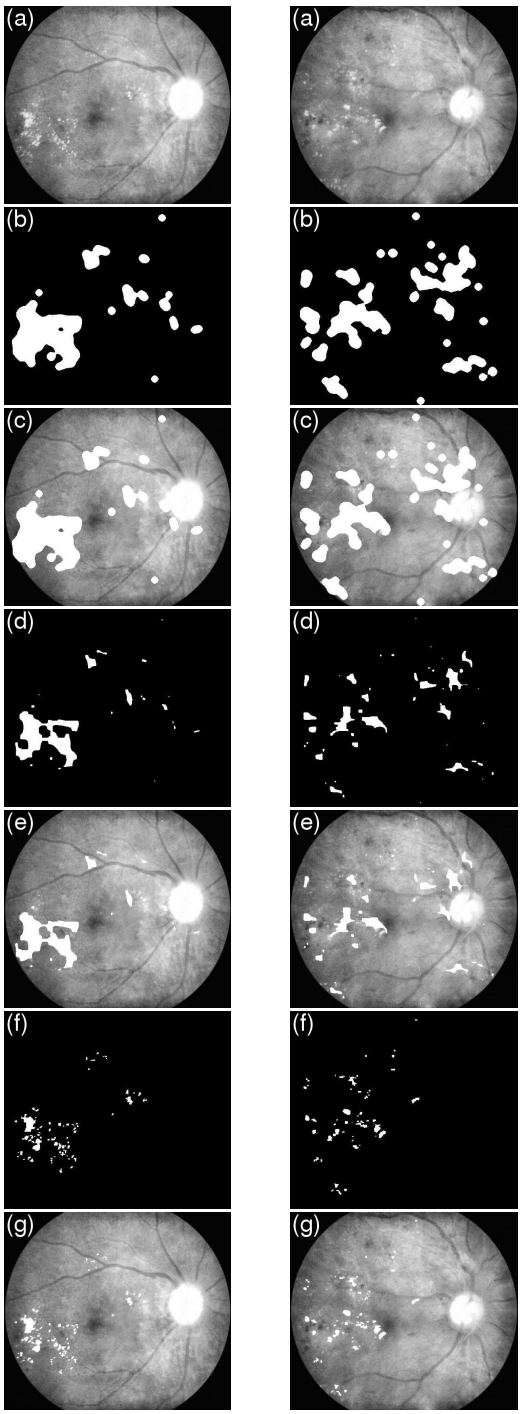

Fig. 12 Example exudates detection results for images 2 (*left*) and 3 (*right*). (a) Intensity image after pre-processing; (b) detected results using subtracted cluster (with $n = 2$); (c) result of (b) superimposed on the original image; (d) detected results using second cluster (with $n = 8$); (e) result of (d) superimposed on the original image; (f) corresponding ground truth images; (g) ground truth superimposed on the original image.

Table 1 PPV and PLR values from exudates detection using the subtracted cluster (top 4 rows) and second cluster (bottom 4 rows) for various n.

n:	2		3		4		5		6		7		8	
	PPV	PLR	PPV	PLR	PPV	PLR	PPV	PLR	PPV	PLR	PPV	PLR	PPV	PLR
Maximum	34.20	32.70	31.11	24.81	29.70	22.15	28.92	20.75	28.37	19.96	28.09	19.52	27.85	19.17
Minimum	0.10	5.35	0.07	4.47	0.07	4.08	0.06	3.89	0.06	3.75	0.06	3.68	0.06	3.63
Average	8.86	13.37	7.23	10.26	6.64	9.20	6.33	8.63	6.14	8.32	6.03	8.12	5.94	7.96
SD	9.45	6.68	8.11	5.12	7.62	4.53	7.37	4.17	7.20	4.02	7.10	3.90	7.03	3.81
Maximum	34.20	32.70	40.29	52.84	46.19	75.44	49.72	93.96	51.37	90.69	53.92	91.32	55.20	93.99
Minimum	0.10	5.35	0.19	6.66	0.27	7.37	0.37	7.72	0.41	7.93	0.49	8.06	0.52	8.15
Average	8.86	13.37	12.22	21.00	14.52	27.07	16.15	32.59	17.41	37.11	18.40	40.82	19.21	44.06
SD	9.45	6.68	11.89	10.87	13.41	15.15	14.40	19.48	15.04	23.36	15.58	26.81	15.94	29.40

Table 2 Averaged performance evaluation results using the subtracted cluster and second cluster.

n	Subtracted cluster				Second cluster			
	Av. Sens. (%)	Av. Spec. (%)	CI of PPV	CI of PLR	Av. Sens. (%)	Av. Spec. (%)	CI of PPV	CI of PLR
2	92.18	91.52	5.93–11.79	11.30–15.44	92.18	91.52	5.93–11.79	11.30–15.44
3	95.45	88.72	4.72–9.74	8.67–11.84	82.87	94.96	8.53–15.90	17.63–24.36
4	96.39	87.37	4.28–9.00	7.80–10.61	76.89	96.24	10.36–18.67	22.38–31.77
5	96.94	86.55	4.04–8.61	7.34–9.92	72.51	96.94	11.69–20.61	26.55–38.62
6	97.07	86.03	3.91–8.37	7.07–9.56	69.16	97.36	12.75–22.07	29.87–44.35
7	97.13	85.72	3.83–8.23	6.92–9.33	66.63	97.65	13.57–23.23	32.52–49.13
8	97.29	85.43	3.76–8.12	6.78–9.14	64.27	97.85	14.26–24.15	34.94–53.17

From these experimental results, the way n is chosen will depend on the application. If the application requires high PPV or PLR, such as an application of an automatic quantitative measurement of exudates, the second cluster with $n = 8$ should be used because it gives a higher accuracy and a low false positive value. However, some applications would not require such a high accuracy, such as an when the method is used as an ophthalmologist's visual aid in exudate detection where the computer enhances the image quality and shows an approximate location of the exudates and the decision is be made by an expert ophthalmologist. In such a case, the subtracted or second cluster with $n = 2$ is recommended since it covers more exudates than the $n = 8$ case. Also, with $n = 2$ the system runs faster.

Future work will address improvement of the performance of this system by finding more specific characteristics of exudates which could distinguish them from other features more effectively. To enhance the FCM clustering algorithm, i.e., improve the sensitivity value with higher true positive value and lower false negative value, morphological techniques might be used in order to obtain more fine-tuned results.

Acknowledgements: We would like to thank the Eye Care Centre, Thammasat University Hospital for supplying the images used in this project. This project was funded by the National Electronics and Computer Technology Centre.

REFERENCES

1. Olson JA, Strachana FM, Hipwell JH, Goatman KA, McHardy KC, Forrester JV, Sharp PF (2003) A comparative evaluation of digital imaging, retinal photography and optometrist examination in screening for diabetic retinopathy. *Diabet Med* **20**, 528–34.
2. Ruamviboonsuk P, Wongcumchang N, Surawongsin P, Panyawatananukul E, Tiensuwan M (2005) Screening for diabetic retinopathy in rural area using single-field, digital fundus images. *J Med Assoc Thai* **88**, 176–80.
3. Sinthanayothin C, Boyce JF, Cook HL, Williamson TH (1999) Automated localisation of the optic disc, fovea, and retinal blood vessels from digital colour fundus images. *Br J Ophthalmol* **83**, 231–8.
4. Sinthanayothin C, Boyce JF, Williamson TH, Cook HL, Mensah E, Lal S, Usher D (2002) Automated detection of diabetic retinopathy on digital fundus images. *Diabet Med* **19**, 105–12.
5. Sanchez CI, Hornero R, Lopez MI, Poza J (2004) Retinal image analysis to detect and quantify lesions associated with diabetic retinopathy. In: IEEE Conference on Engineering in Medicine and Biology Society, vol 1, pp 1624–7.
6. Hsu W, Pallawala PMDS, Lee ML, Au Eong KG (2001) The role of domain knowledge in the detection of retinal hard exudates. In: IEEE Computer Society Conference on Computer Vision and Pattern Recognition, vol 2, pp 246–51.
7. Gardner GG, Keating D, Williamson TH, Elliot AT (1996) Automatic detection of diabetic retinopathy using an artificial neural network: a screening tool. *Br J Ophthalmol* **80**, 940–4.

8. Wang H, Hsu W, Goh KG, Lee ML (2000) An effective approach to detect lesions in color retinal images. In: Proceedings of the IEEE Conference on Computer Vision and Pattern Recognition, vol 2, pp 181–6.
9. Walter T, Klein J-C, Massin P, Erginay A (2002) A contribution of image processing to the diagnosis of diabetic retinopathy-detection of exudates in color fundus images of the human retina. *IEEE Trans Med Imag* **21**, 1236–43.
10. Phillips RP, Forrester J, Sharp P (1993) Automated detection and quantification of retinal exudates. *Graefe's Arch Clin Exp Ophthalmol* **231**, 90–4.
11. Huiqi Li Chutatape O (2003) A model-based approach for automated feature extraction in fundus images. In: Proceedings of 9th IEEE International Conference on Computer Vision, vol 1, pp 394–9.
12. Usher D, Dumskyj M, Himaga M, Williamson TH, Nussey S, Boyce J (2004) Automated detection of diabetic retinopathy in digital retinal images: a tool for diabetic retinopathy screening. *Diabet Med* **21**, 84–90.
13. Kavitha D, Devi SS (2005) Automatic detection of optic disc and exudates in retinal images. In: Conference on Intelligent Sensing and Information Processing, pp 501–6.
14. Goh KG, Hsu W, Lee ML, Wang H (2001) ADRIS: an automatic diabetic retinal image screening system. In: Cios KJ (ed) *Medical Data Mining and Knowledge Discovery*, Physica-Verlag, Heidelberg, pp 181–210.
15. Ege BM, Hejlese OK, Larsen OV, Moller K, Jennings B, Kerr D, Cavan DA (2000) Screening for diabetic retinopathy using computer based image analysis and statistical classification. *Comput Meth Programs Biomed* **62**, 165–75.
16. Wang X, Wang Y, Wang L (2004) Improving fuzzy c-means clustering based on feature-weight learning. *Pattern Recogn Lett* **25**, 1123–32.
17. Siyal MY, Lin Yu (2005) An intelligent modified fuzzy c-means based algorithm for bias estimation and segmentation of brain MRI. *Pattern Recogn Lett* **26**, 2052–62.
18. Chuang KS, Tzeng HL, Chen S, Wu J, Chen TJ (2006) Fuzzy c-means clustering with spatial information for image segmentation. *Comput Med Imag Graph* **30**, 9–15.
19. Dunn JC (1973) A fuzzy relative of the ISODATA process and its use in detecting compact well-separated clusters. *J Cybern* **3**, 32–57.
20. Bezdek JC (1981) *Pattern Recognition with Fuzzy Objective Function Algorithms*, Plenum Press, New York.
21. Osareh A, Mirmehdi M, Thomas B, Markham R (2001) Automatic recognition of exudative maculopathy using fuzzy c-means clustering and neural networks. In: Proceedings of the Medical Image Understanding Analysis Conference, pp 49–52.
22. Osareh A, Mirmehdi M, Thomas B, Markham R (2003) Automated identification of diabetic retinal exudates in digital colour images. *Br J Ophthalmol* **87**, 1220–3.
23. Osareh A, Mirmehdi M, Thomas B, Markham R (2002) Classification and localisation of diabetic-related eye disease. In: Proceedings of the 7th European Conference on Computer Vision, vol 4, pp 502–16.
24. Osareh A, Mirmehdi M, Thomas B, Markham R (2002) Comparative exudate classification using support vector machines and neural networks. In: *Medical Image Computing and Computer-Assisted Intervention – MICCAI 2002*, Springer, Berlin, pp 413–20.
25. Zhang X, Chutatape O (2005) Top-down and bottom-up strategies in lesion detection of background diabetic retinopathy. In: IEEE Computer Society Conference on Computer Vision and Pattern Recognition, vol 2, pp 422–8.
26. Feman SS, Leonard-Martin TC, Andrews JS, Armbruster CC, Burdge TL, Debelak JD, Lanier A, Fischer AG (1995) A quantitative system to evaluate diabetic retinopathy from fundus photographs. *Investig Ophthalmol Vis Sci* **36**, 174–81.
27. Gonzales RC, Woods RE (2002) *Digital Image Processing*, 2nd edn, Addison-Wesley, NJ, pp 65–107.
28. Gillespie AR, Kahle AB, Walker RE (1986) Color Enhancement of Highly Correlated Images. I. Decorrelation and HIS Contrast Stretch. *Rem Sens Environ* **20**, 209–35.
29. Phung SL, Bouzerdoum A Sr, Chai D Sr (2005) Skin segmentation using color pixel classification: Analysis and comparison. *IEEE Trans Pattern Anal Mach Intell* **27**, 148–54.
30. Wang XY, Garibaldi J, Ozen T (2003) Application of the fuzzy C-means clustering method on the analysis of non pre-processed FTIR data for cancer diagnosis. In: Conference on Australian and New Zealand Intelligent Information Systems, pp 233–8.
31. Musa H, Alci M (2005) Reliability analysis of microarray data using fuzzy c-means and normal mixture modeling based classification methods. *Bioinformatics* **21**, 644–9.
32. Kallergi M (2005) Evaluation strategies for medical-image analysis and processing methodologies. In: Costaridou L (ed) *Medical Image Analysis Methods*, Taylor and Francis Group CRC Press, Florida, pp 433–71.
33. Attia J (2003) Moving beyond sensitivity and specificity: using likelihood ratios to help interpret diagnostic tests. *Aust Prescriber* **26**, 111–3.